Comparative growth study of ultrathin Bi films on clean and oxygen-reconstructed Nb(110)

Robin Boshuis [1,*] Artem Odobesko [1], Felix Friedrich [1], Johannes Jung,[1] and Matthias Bode [1,2]

[1]*Physikalisches Institut, Experimentelle Physik II, Universität Würzburg and Würzburg-Dresden Cluster of Excellence ct.qmat, Am Hubland, 97074 Würzburg, Germany*

[2]*Wilhelm Conrad Röntgen-Center for Complex Material Systems (RCCM), Universität Würzburg, Am Hubland, 97074 Würzburg, Germany*

We present a detailed study of the growth of Bi films on superconducting Nb(110) substrates in dependence on the Bi coverages and the Nb surface quality. We find that Bi grows in a (110) orientation at low coverage equivalent to about five pseudomorphic monolayers (ML^{ps}) on clean Nb(110), but then undergoes a structural transition to Bi(111) below about 8 ML^{ps}. Comparison with two oxygen-reconstructed Nb(110) surfaces, the NbO_x phases I and II, reveals that the film thickness at which the (110)-to-(111) transition takes place depends on the surface quality. Whereas it is observed at lower coverage for the NbO_x phase I, our results indicate that Bi(110) remains stable on NbO_x phase II up to the largest film thickness studied here, i.e., 18 ML. The quality and smoothness of the thin Bi films considerably depends on the cleanliness of the Nb substrate, revealing the most flat and defect-free Bi films grown on the oxygen-free clean Nb(110) surface.

I. INTRODUCTION

Due to the increased interest in material systems suitable for fault-tolerant quantum computing, topological superconductors have gained wide interest in recent years [1,2]. Towards this goal, thin Bi films on superconducting substrates have been discussed as a potential material system [3]. Elemental Bi has often been considered as a topological nontrivial material. It was theoretically predicted that the free-standing bilayer (BL) of strongly spin-orbit–coupled Bi(111) is a two-dimensional (2D) topological insulator [4–6]. The experimental detection of topological edge states in thin Bi films on Bi_2Te_3 and Bi_2Se_3 confirmed this prediction [7,8]. Furthermore, it has been reported that honeycomb structures of Bi on SiC(0001) exhibit topological edge modes [9]. Later, it was shown that bilayer Bi(111) islands atop a bulk Bi crystal also host topologically nontrivial edge states localized at surface hinges [10,11]. Efforts to grow Bi(111) on surfaces of superconductors, such as $NbSe_2$ [12] and Nb(110) [3,13], confirmed its topological nature and revealed a proximity-induced superconducting state.

Previous theoretical and experimental studies have shown that ultrathin epitaxial Bi films grow either in the (111) or in the (110) orientation on most substrates. Several studies consistently indicated that the Bi film thickness plays a decisive role in what orientation the film adopts. Experiments performed on various substrates, such as $TiSe_2$ [14], Si(111) [15], HOPG [16], Ge(111) [17], or $NbSe_2$ [18] suggest a common scenario where ultrathin films with a thickness of a few nanometers grow in the Bi(110) orientation, whereas thicker films preferably form a Bi(111) surface.

In contrast, Nb surfaces which are exceedingly difficult to clean from oxygen [19,20] have not yet been investigated systematically. Nb is a type-II superconductor with the high-est superconducting transition temperature $T_c = 9.2$ K of all elements and a large coherence length $\xi = 38$ nm. Therefore, it is a favorable choice for the experimental investigation of a proximity-induced superconducting state in topologically nontrivial materials. Recently we showed that the chemical composition and structural perfection of the Nb(110) surface is determined by the temperature at which Nb is heated during preparation [21]. While a temperature close to the Nb melting point is required to obtain clean Nb(110), lower preparation temperatures result in two oxygen-induced reconstructions.

In this work we present a detailed investigation of the growth of Bi thin films on various clean and oxygen-reconstructed Nb(110) surfaces. Regardless of the presence or absence of surface reconstructions we find that Bi grows in the (110) orientation at low coverage. Our results reveal, however, that the question of whether Bi exhibits a structural transition from (110)- to (111)-oriented films and, if so, at which critical thickness this transition occurs, strongly depends on the quality of the underlying Nb substrate. This discovery not only allows us to intentionally tune the film symmetry, it also reveals that future investigations of potential topological superconducting properties may be performed with Bi films as thin as 2 BL, thereby offering particularly strong proximity-induced superconductivity.

II. NOMENCLATURE

To describe the films grown in this work, we use the rhombohedral notation, as its unit cell is the primitive unit cell of the bulk crystal [22]. Figure 1 displays a ball-and-stick model of two Bi surfaces relevant in the context of this contribution. The Bi(111) surface consists of two sublattices, marked in blue and cyan in Fig. 1(a), which both exhibit a hexagonal lattice. Red sticks represent the rhombohedral primitive unit cell. The blue spheres form three distinct layers, where the top and bottom layers are equivalent, with a distance of $3h_{Bi(111)} = 11.79$ Å between each other. The layers formed
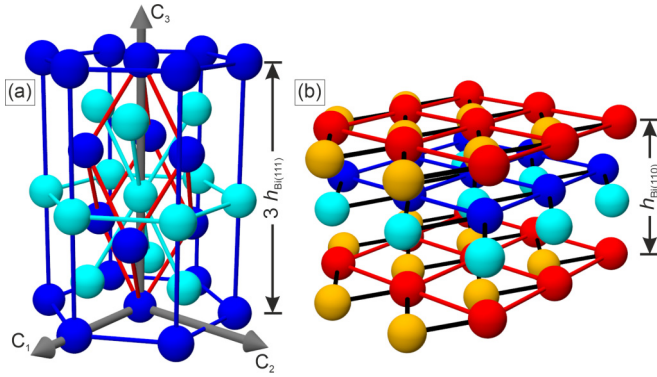
FIG. 1. Ball-and-stick model of (a) the (111)- and (b) the (110)-terminated Bi surfaces in respect to the bulk crystal lattice. The characteristic interlayer distances $3h_{Bi(111)}$ and $h_{Bi(110)}$ are indicated by black arrows, respectively.

by cyan spheres are interlaced between blue layers and have the same crystal lattice, but are vertically shifted from the position in the center between two blue layers. This results in a ratio of the distances of a given cyan layer to the blue layers below and above, d_1 and d_2, respectively, that amounts to $d_2/d_1 = 0.88$. As a consequence, a Bi(111) bilayer consists of a blue and a cyan plane with a total nominal bilayer height $h_{Bi(111)} = 3.93$ Å.

Since the (110) plane of the Bi crystal lattice can hardly be recognized in this representation, Fig. 1(b) shows the same bulk crystal lattice which is now terminated by a (110) surface. The atoms marked orange are not only shifted within the plane slightly away from the position in the center of the red rectangle, but also exhibit a very small out-of-plane displacement. For better visibility, this displacement has been enhanced in Fig. 1(b). In reality, the out-of-plane corrugation is as low as 0.14 Å [23]. In this respect, the height of a bilayer (BL) is defined as the distance between two red layers, the bilayer therefore consisting of two buckled monolayers (red/orange and blue/cyan). Therefore, the calculated BL height of the Bi(110) surface amounts to $h_{Bi(110)} = 6.81$ Å.

Obviously, the number of atoms per area is not the same for Bi(110) and Bi(111) bilayers. Throughout this paper, we define the amount of Bi deposited on the substrate with respect to the substrate lattice of clean Nb(110), i.e., a pseudomorphic monolayer (ML^{ps}) corresponds to one Bi atom for each Nb substrate surface atom. Please note, that—according to our results presented below—Bi never really grows pseudomorphic on Nb(110), but forms either (110)- or (111)-terminated films. Therefore, we will be using ML^{ps} to describe the *nominal* amount of deposited material. With this definition, we can describe the conversion from ML^{ps} to Bi bilayers in (111) and (110) orientation. Hereby, one bilayer Bi(111) (1 BL^{111}) holds the same number of atoms per surface area as 0.86 ML^{ps}, while one bilayer Bi(110) (1 BL^{110}) is the equivalent to 1.43 ML^{ps}. For a more detailed description of the Bi crystal lattice and surfaces, see Ref. [22].

III. METHODS

The study has been performed in a UHV system (base pressure $p \approx 5 \times 10^{-11}$ mbar) which is equipped with a low-energy electron diffraction (LEED) optics and a variable-

temperature scanning tunneling microscope (STM). By feeding cold nitrogen gas through the flow cryostat we reach a base sample temperature $T_{STM} = 122$ K while the tip and the tube scanner remain at room temperature.

The Nb(110) crystal is initially prepared by cycles of Ar^+–ion sputtering and heating by electron bombardment. As described in Ref. [21], an oxygen-free (clean) Nb surface can be achieved by numerous high-temperature flashes at $T_{fl} > 2400°C$. In contrast, oxygen-reconstructed surfaces are obtained when lower flash temperatures are applied: At $T_{fl} \lesssim 2000C$ the surface forms an chainlike oxygen-induced reconstruction (called phase I in the following); for a flash temperature $T_{fl} \gtrsim 2000C$ the Nb surface exhibits another, higher ordered oxygen-induced reconstruction (phase II) [24]. This phase II is characterized by extended patches of oxygen rows oriented along the $[\bar{1}12]$ and the $[\bar{1}1\bar{2}]$ direction.

Bismuth is deposited by thermal evaporation of high-purity material (Alfa Aesar, 99.999%) from a quartz glass crucible. The deposition rate amounts to approximately 0.7 ML^{ps} per minute (see Sec. II for details). To minimize the formation of stacking faults and crystallographic grains the substrate is cooled to $T_{dep} \approx 180$ K during deposition [13]. After Bi deposition the sample is annealed at about $200C \leqslant T_{ann} \leqslant 240C$ for 5 min [24].

Details of the STM image processing can be found in the Supplemental Material [24]. For better visibility of our STM data, the z signal recorded in the topographic constant-current image was augmented by its derivative with respect to the fast scan direction, dz/dx. Depending on the maximal corrugation, the exact mixing ratio of z and dz/dx varies for different images of this study. As a result, the color-code cannot directly be interpreted as a height information. Wherever necessary, line profiles will be presented to allow for a quantitative assessment.

IV. RESULTS

A. Bi growth on clean Nb(110)

In Fig. 2 we present overview constant-current STM images (scan range 1 μm × 1 μm) and LEED data of Bi films grown on clean Nb(110). The respective Bi coverage amounts to (a) 1.2 ML^{ps}, (b) 4.7 ML^{ps}, and (c) 8.3 ML^{ps}. At the lowest coverage, Fig. 2(a), islands with a typical diameter of about 100 nm which cover about 43% of the total surface area can be recognized. Almost all islands exhibit a height of (13.4 ± 0.7) Å, corresponding to 2 BL^{110}. The shape of the islands is similar to isogonal octagons with D_4 symmetry, as indicated for one island in the center of Fig. 2(a). The short edges of these octagons are oriented along the [0 0 1] and [1 $\bar{1}$ 0] directions and the long edges along the [2 $\bar{2}$ 3] and [2 $\bar{2}$ $\bar{3}$] directions of the Nb(110) substrate. The reason for these rather uncommon growth directions will be discussed below.

The LEED pattern of this sample is presented in the lower right of Fig. 2(a). In addition to the spots of clean Nb(110) which are marked by blue squares, we recognize three weaker diffraction spots in between the Nb(110) spots along the [1 $\bar{1}$ 0] direction (red pentagons). Furthermore, very weak spots indicative of a Bi(110) surface are observed (green circles) [25].
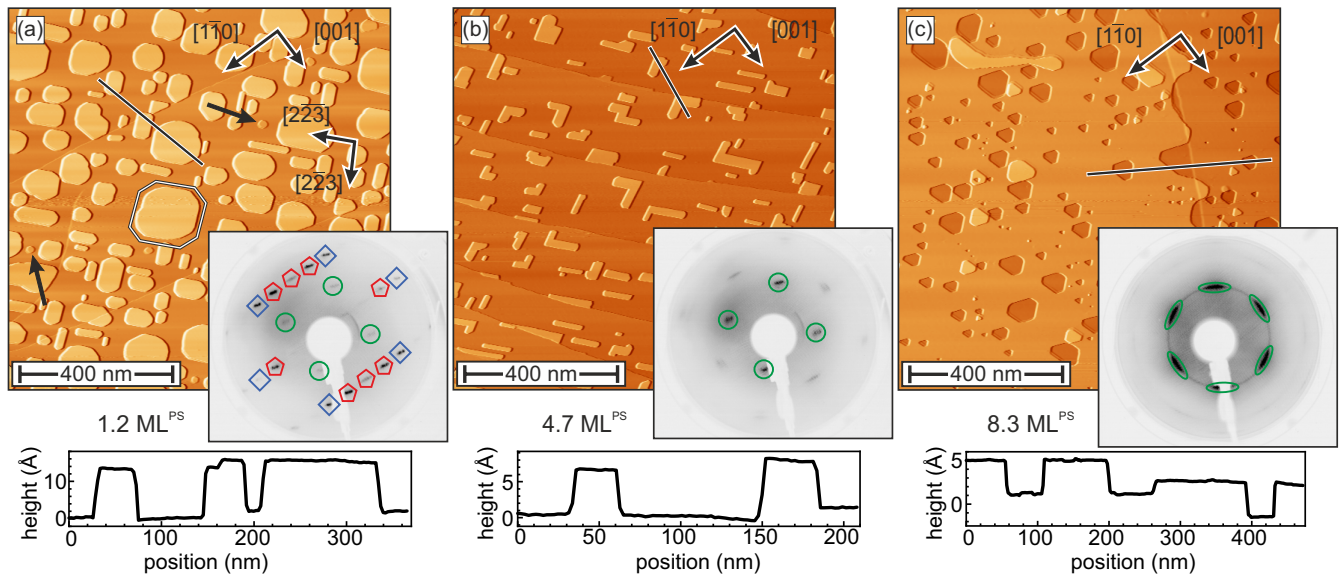
FIG. 2. STM topographic images (left) and LEED patterns (bottom right) of Bi films grown on clean Nb(110) at coverages of (a) 1.2 ML^{ps} of Bi, (b) 4.7 ML^{ps}, and (c) 8.3 ML^{ps}, respectively. Irrespective of the particular coverage, the STM data confirm that Bi film growth proceeds in a layer-by-layer fashion. The LEED patterns are indicative of film thickness-dependent structural changes. While a pronounced superstructure can be recognized at 1.2 ML^{ps}, the LEED patterns observed at 4.7 ML^{ps} and 8.3 ML^{ps} are characteristic for the Bi(110) and Bi(111) surface. Scan parameters: $U = -1$ V, $I = 100$ pA; LEED: (a) $E = 75$ eV, (b) $E = 70$ eV, (c) $E = 80$ eV.

As sketched in Fig. 3, the red-marked superstructure spots observed in the LEED pattern of Fig. 2(a) can consistently be explained by a Bi wetting layer with atomic positions corresponding to a distorted Bi(110) monolayer. Due to the much lower surface free energy of Bi as compared to Nb [26], the existence of a wetting layer can readily be expected. In our model the Bi atoms alternatingly occupy two threefold coordinated hollow sites and one on-top site of Nb(110). We speculate that the vertical displacement caused by adsorption of Bi atoms in these distinct surface sites is much larger than
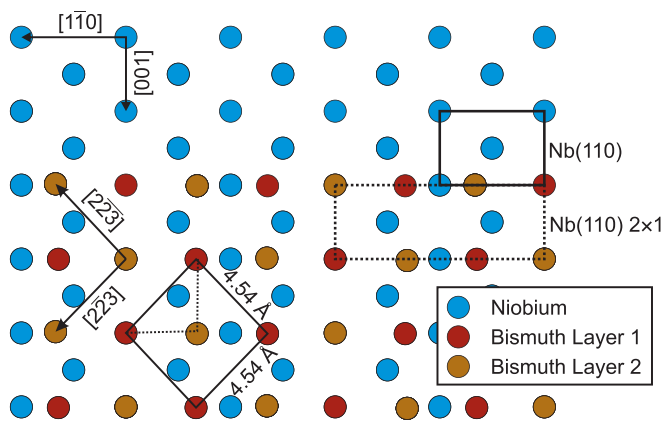

FIG. 3. Model of the Bi wetting layer on clean Nb(110). The atoms of the Nb(110) surface layer are represented by blue dots. Red and orange dots mark the two sublattices of a buckled Bi(110) monolayer. The atoms alternatingly occupy two threefold coordinated hollow sites and one on-top site. The 2×1 unit cell (hatched rectangle) underlying the LEED pattern observed in Fig. 2(a) can be explained if the adsorption site-dependent corrugation of the wetting layer is much larger than the buckling intrinsic to the Bi(110) monolayer.

the subtle vertical distance between the two atomic planes within a buckled Bi(110) monolayer. Therefore, the distinction between these two layers, which are shown as orange and red dots in Fig. 3, becomes irrelevant, resulting in a rectangular (2×1) unit cell with nominal dimensions of 3.30 Å and 9.33 Å along the Nb [0 0 1] and [1 $\bar{1}$ 0] directions, respectively.

The epitaxial relationship sketched in Fig. 3 aligns the in-plane [0 1 0] and [1 0 $\bar{1}$] directions of the Bi(110) film along the [2 $\bar{2}$ 3] and [2 $\bar{2}$ $\bar{3}$] directions of the Nb(110) substrate, i.e., the island edges visible in Fig. 2(a) are indeed oriented along the film's high-symmetry directions. The resulting interatomic spacing of about 4.54 Å closely matches the nominal in-plane Bi(110) lattice constants of 4.54 Å and 4.75 Å with a relatively low uniaxial compressive strain $s \approx (a_{Nb} - a_{Bi_{nnn}})/a_{Bi_{nnn}} = -6.6\%$. We would like to note, however, that the 4.54 Å × 4.54 Å cell sketched in Fig. 3 is not perfectly rectangular but exhibits a slightly tilted parallelogram, the tilt direction of which alternates between adjacent cells. On top of this wetting layer we find islands with a height expected for two BL^{110}, $h = 13.6$ Å. Only very occasionally some islands with a height consistent with a single bilayer and a typical diameter of about 10 nm are observed, two of which are marked by black arrows in Fig. 2(a). These (110)-terminated Bi islands cause the diffraction spots marked green in the LEED pattern of Fig. 2(a).

As the Bi coverage is increased to 4.7 ML^{ps} [see Fig. 2(b)], we still recognize atomically flat terraces separated by single-atomic step edges of the Nb(110) substrate. On top of these terraces we find islands with edges preferentially aligned along the substrate's [2 $\bar{2}$ 3] and [2 $\bar{2}$ $\bar{3}$] directions. The corresponding LEED data show a pattern qualitatively consistent with a Bi(110) surface. No traces of the (2×1) unit cell of the Bi wetting layer on Nb(110) can be found anymore, indicating that the entire film now exhibits a Bi(110) structure.

At a Bi coverage of 8.3 ML^{ps} [see Fig. 2(c)], the film remains atomically flat. However, we observe a fundamentally different film morphology. Only few, hexagon-shaped adislands and vacancy islands with a typical diameter of tens of nm can be found. This island shape suggests a Bi-vacuum interface which is no longer terminated by a (110) but instead by a (111)-oriented Bi surface. Correspondingly, the islands exhibit a height of $h = (3.9 \pm 0.4)$ Å, equivalent to 1 BL^{111}. As can be seen in the bottom panel of Fig. 2(c), the LEED pattern of this surface shows six diffraction maxima which are rotated by 60° with respect to each other, in agreement with the lattice symmetry expected for Bi(111) [22]. The planar epitaxial relationship can be described by a binary (C_2) axis of Bi(111) [cf. directions defined in Fig. 1(a)] which is roughly oriented along the [1$\bar{1}$0] direction of Nb(110). However, the spots profiles are not dot shaped but rather form circular arcs.

We interpret this finding as evidence for a Bi(111) film which is not single crystalline but consists of numerous grains which correspond to rotational domains. We assume that the diameter of the focused electron beam is much larger ($>250\,\mu$m according to the manufacturer's specifications) than the grain size. Therefore, the LEED pattern represents numerous Bi(111) grains, the binary (C_2) axes of which somewhat vary in orientation around the Nb [1$\bar{1}$0] direction. The scan range of typical STM images, in contrast, is apparently much smaller than the grain size. Therefore, they show the surface structure of a single Bi(111) grain only.

The results of this section show that smooth Bi films with wide atomically smooth terraces, few atomic step edges, and regularly shaped islands can be grown on clean Nb(110) by low-temperature deposition and subsequently annealing at $200\,°\text{C} \leqslant T_{\text{sample}} \leqslant 240\,°\text{C}$. Our STM and LEED data also reveal that the film orientation changes with film thickness. Whereas Bi(110) films were observed up to 4.7 ML^{ps}, we find a (111)-oriented Bi surface for films with 8.3 ML^{ps} coverage. We will see below, that the thickness where the transition from (110)- to (111)-oriented Bi films occurs depends on the quality of the Nb substrate, as very different values are found for oxygen-reconstructed Nb(110) surfaces.

B. Bi growth on oxygen-reconstructed Nb(110)

Figures 4(a) and 4(b) show STM and LEED data of Bi films with 4.7 ML^{ps} coverage grown on the NbO$_x$ phase II and the NbO$_x$ phase I surface reconstruction, respectively. For the NbO$_x$ phase II in Fig. 4(a) we observe a very smooth, completely closed Bi(110) film. Only very few small, rectangular-shaped islands can be recognized. These islands have a well-defined height of about (6.15 ± 0.62) Å, in good agreement with 1 BL^{110}. A (110)-terminated Bi surface is also confirmed by the atomic resolution STM data presented in the upper right panel of Fig. 4(a). We find lattice constants of 4.05 Å and 4.96 Å which somewhat deviate from the literature values of (110)-terminated Bi, 4.54 Å and 4.75 Å. Since the STM data may, however, be influenced by thermal drift or piezo creep, we are currently not able to determine the strain of these Bi films. The (110) surface orientation of the Bi film on the NbO$_x$ phase II is also corroborated by the twofold symmetric LEED pattern presented in the lower right panel of Fig. 4(a). Both the STM and LEED data consistently show
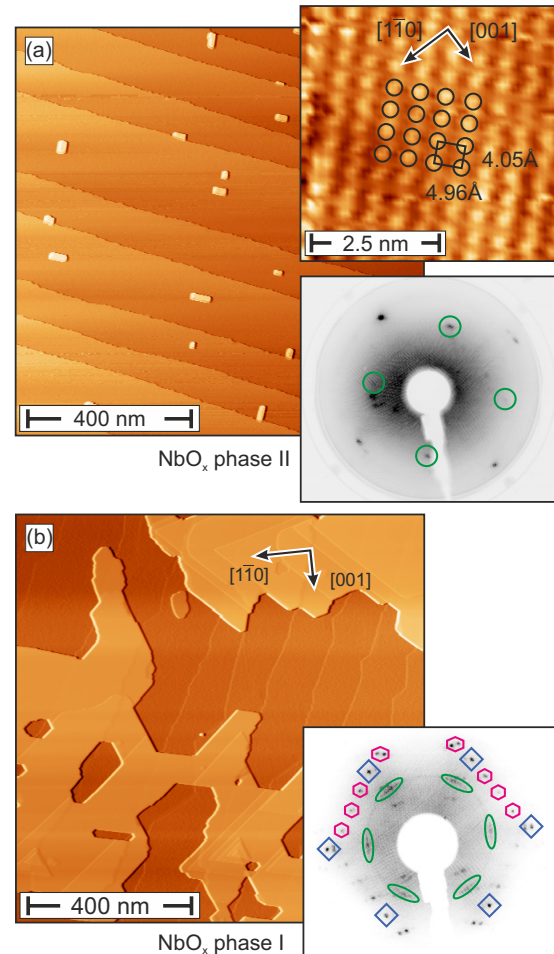

FIG. 4. STM topographic images (left) and LEED patterns (bottom right) of Bi films with a coverage of 4.7 ML^{ps} on different oxygen-reconstructed surfaces of Nb(110): (a) NbO$_x$ phase II and (b) NbO$_x$ phase I. The film grown on NbO$_x$ phase II is very flat and exhibits the LEED pattern of Bi(110) ($E = 36$ eV). This is also confirmed by the atomic resolution STM data presented in the upper right panel of (a). In contrast, the Bi film grown on NbO$_x$ phase I shows pronounced island growth, triangularly shaped islands, and sixfold-symmetric LEED spots, indicative of a Bi(111) structure ($E = 90$ eV). Scan parameters: $U = -1$ V, $I = 100$ pA for overview images; $U = -100$ mV, $I = 100$ pA for atomic resolution.

that the Bi(110) lattice is rotated by about 45° with respect to the underlying Nb(110) substrate.

Even superficial inspection of the data of a Bi film with a coverage of 4.7 ML^{ps} grown on the NbO$_x$ phase I, displayed in Fig. 4(b), indicates a completely different growth mode than the one observed for phase II. First, the overview STM image clearly shows that the Bi no longer covers the entire substrate but instead forms separate patches. Between the patches a step-and-terrace structure reminiscent to the underlying Nb(110) substrate can be recognized. Second, triangular islands can be recognized on the Bi patches, indicating a (111) surface orientation. The height of these islands and other step edges on the Bi patches amounts to about (3.83 ± 0.28) Å, in good agreement with 1 BL^{111}. Finally, the LEED pattern presented in the lower right panel of Fig. 4(b) is rather complex. Detailed analysis reveals that it consists of spots originating
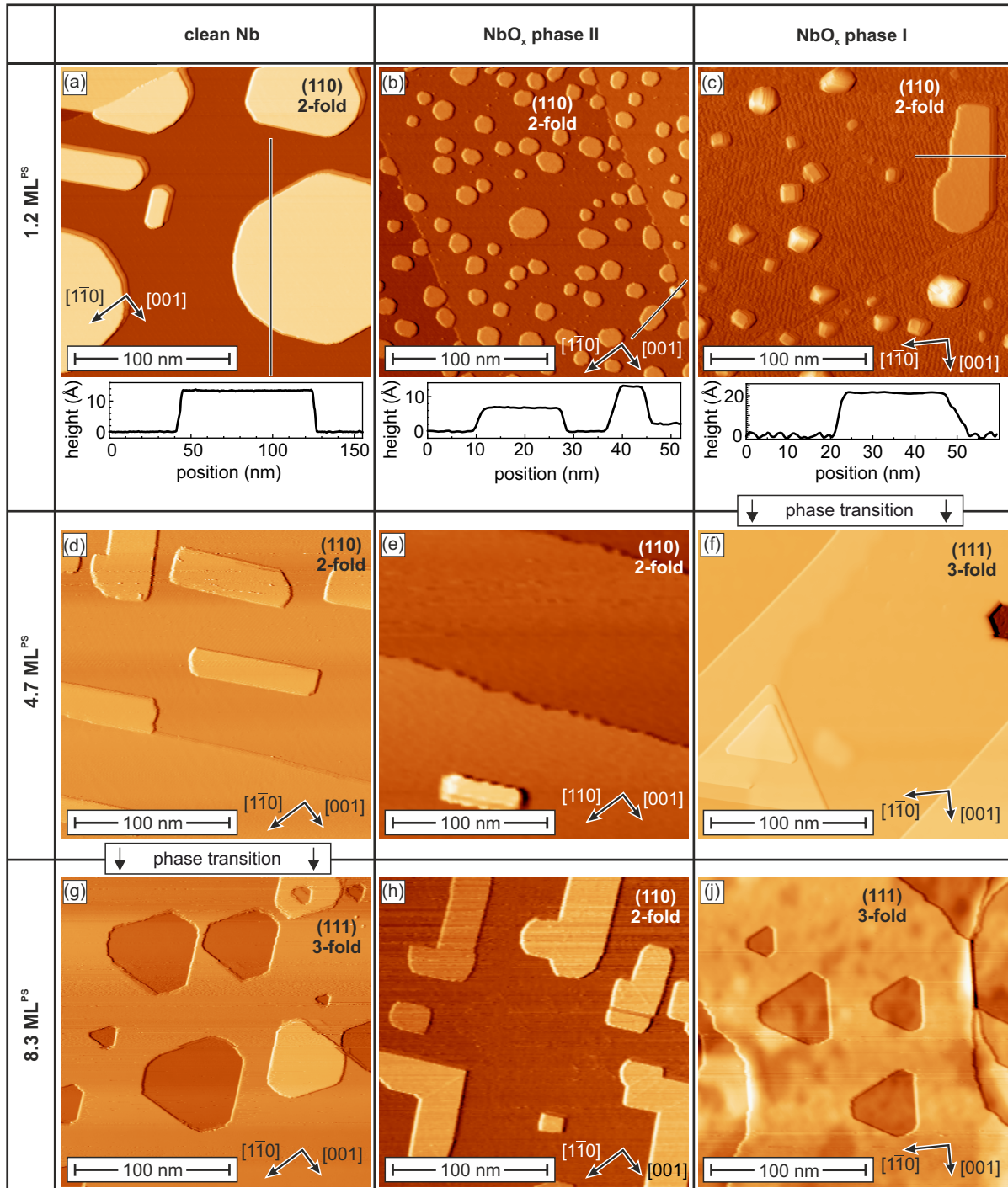
FIG. 5. STM topography images of Bi on Nb(110). STM scan parameters: $U = -1$ V, $I = 100$ pA. Each column shows a different surface quality of the Nb(110) substrate, each row a certain amount of deposited Bi material: (a)–(c) 1.2 ML^{ps} of Bi; (d)–(f) 4.7 ML^{ps}; and (g)–(j) 8.3 ML^{ps}. The symmetry of the Bi surface is noted in the upper right corner of each panel. Phase transitions from (110)- to (111)-oriented Bi are indicated.

from the Nb(110) lattice (marked by blue squares), from the NbO$_x$ phase I reconstruction (magenta hexagons) [21], and an inner ring of six circularly broadened spots characteristic for Bi(111), similar to those observed for a much higher Bi coverage on clean Nb(110); cf. Fig. 2(c).

These data suggest that the coverage at which the transition from (110)- to (111)-oriented Bi occurs sensitively depends on the structural and chemical properties of the particular

Nb(110) substrate. In the following section we will present a more detailed comparison.

C. Substrate dependence of critical coverage

Figure 5 presents a table of overview topographic STM images displaying the evolution of Bi films grown on Nb(110) crystals with various surface qualities. From left to right, the

columns show data obtained on the the oxygen-free, clean Nb surface, the NbO_x phase II, and on the NbO_x phase I [24]. On each of these Nb surfaces Bi films were grown as described in Sec. III above. The rows, from top to bottom, show typical results obtained for Bi coverages of 1.2 ML^{ps}, 4.7 ML^{ps}, and 8.3 ML^{ps}, respectively.

First, we want to discuss the STM data presented in the first row for low Bi coverages of about 1.2 ML^{ps} [Figs. 5(a)–5(c)]. Independent of the particular surface quality, all three topographic images are governed by Bi islands. As can be seen in the line profiles which were measured along the black lines in Figs. 5(a)–5(c) and which are plotted in the bottom of the respective panel, the island heights agree well with multiples of 1 BL^{110}. The island edge orientation is either along the [001] and the [1$\bar{1}$0] direction or rotated by about 45°. Based on these observations we conclude that at a coverage of 1.2 ML^{ps} Bi grows in a (110) orientation on all Nb(110) surfaces considered here.

However, there also exist significant differences between clean Nb(110) and the two oxygen-reconstructed surfaces. On the clean Nb(110) surface, Fig. 5(a), the Bi islands are much more extended than on oxidized Nb. This is a first hint towards an increased mobility of the Bi atoms on the oxygen-free Nb surface during the annealing process. These islands have a size of up to 150 nm, mostly a height of 2 BL^{110}, and exhibit well-defined straight edges.

Inspection of Bi islands on the NbO_x phase II, displayed in Fig. 5(b), reveals a height of 1 BL^{110}. Only very few Bi islands with a local coverage of 2 BL^{110} were found, one of which is analyzed by the line profile displayed in the bottom panel of Fig. 5(b). These islands are roughly round shaped with a diameter between 10 and 30 nm. On the NbO_x phase I, in addition to the flat island which appears in the upper right corner of Fig. 5(c) with a height of approximately 3 BL^{110}, numerous clusters can be observed. The lateral extension of these clusters is very small, typically about 10–20 nm, whereas the flat island mentioned above has a length of up to 90 nm along the [001] direction. In between these islands, a wetting layer can be recognized which is characterized by stripes the periodicity and orientation of which is consistent with the NbO_x phase I oxygen reconstruction [24].

Data obtained on 4.7 ML^{ps} Bi films on the various Nb surfaces are presented in the second row [Figs. 5(d)–5(f)]. As stated previously in Secs. IV A and IV B, we find completely closed Bi(110) films with small, mostly rectangular shaped islands on the clean Nb(110) surface and on the NbO_x phase II; see Figs. 5(d) and 5(e), respectively. The height of these islands corresponds to the height of 1 BL^{110}, and the island edges are preferentially oriented along the [2$\bar{2}$3] and the [2$\bar{2}\bar{3}$] directions of the Nb substrate. In contrast, for the NbO_x phase I we find triangularly shaped islands with a height equivalent to 1 BL^{111} [see Fig. 5(f)]. These results imply that the Bi film on NbO_x phase I undergoes a phase transition from (110) to (111) at a Bi coverage between 1.2 and 4.7 ML^{ps}.

The STM data of Figs. 5(g)–5(j) display the film morphology after depositing 8.3 ML^{ps} Bi on clean Nb(110), the NbO_x phase II, and the NbO_x phase I, respectively. At this coverage, we now also find threefold-symmetric Bi adislands and vacancy islands on clean Nb(110) [see Fig. 5(g)]. Their step heights match 1 BL^{111}. We conclude that between 4.7 ML^{ps}

and 8.3 ML^{ps} the epitaxial relation between the clean Nb(110) substrate and the Bi film must have changed from the twofold Bi(110) to the threefold Bi(111) surface.

In contrast, we observe no hints for such a phase transition for the growth of Bi on the NbO_x phase II. The data of Fig. 5(h) still show rectangular islands, indicating the prevalence of a (110)-oriented Bi surface. Even when the deposited Bi amount was increased to 17.8 ML^{ps}, the Bi(110) order remained [24]. For 8.3 ML^{ps} Bi on the NbO_x phase I, Fig. 5(j), we find that the film maintains its threefold (111) symmetry. Even though step edges and atomically flat terraces are clearly visible, the STM topographic data of Fig. 5(j) reveal an uneven, "bumpy" surface. This impression is caused by the fact that the atomically flat terraces are not completely even but exhibit—on typical length scales of 10 nm—a corrugation of 1–2 Å, i.e., well below the height of a monatomic step edge. Since the film surface of the 4.7 ML^{ps} film previously presented in Fig. 5(f) was much smoother, we can safely exclude that the cluster growth process which we observed at very low Bi coverage [cf. Fig. 5(c)] is responsible for this bumpiness. Potentially, the corrugation of the film surface is caused by the elimination of stacking faults by gliding, as observed previously for rare-earth metal films when stacking faults eventually heal at large film thickness [27].

V. DISCUSSION

For Bi grown on clean Nb(110) and on the NbO_x phase I substrate we observe a structural transition from twofold Bi(110)-oriented films at low Bi coverage to the threefold Bi(111) surface at higher coverage. A similar transformation of Bi films was observed previously on $TiSe_2$ [14], Si(111)-7 × 7 [15], HOPG [16], Ge(111) [17], or $NbSe_2$ [18]. However, on Nb a wider range of scenarios occurs. At very low coverage Bi tries to adopt the twofold symmetry of the Nb(110) substrate through a (2 × 1) reconstruction of the centered unit cell. This reconstruction can be verified by LEED measurements of 1.2 ML^{ps} on clean Nb(110). The lattice of this Bi(110)-2 × 1 lattice matches very well the bulk Bi(110) unit cell size with a strain of approximately −6.6%.

Whereas we find the (110)-to-(111) transition between 1.2 ML^{ps} and 4.7 ML^{ps} for phase I-terminated NbO_x substrates, it is delayed to between 4.7 and 8.3 ML^{ps} for clean Nb(110). Surprisingly, no such transition can be observed for the NbO_x phase II, where (110)-oriented Bi films prevail up to the highest Bi coverages studied here, i.e., about 18 ML^{ps}. It is quite reasonable to assume and in agreement with existing literature [22] that the structural phase transition at higher coverages originates from an energy gain of (111)-terminated Bi in comparison with Bi(110) films. At very thin film thickness, it is overcompensated by the bond of Bi with the substrate and by the lower film strain. On the clean Nb surface, apparently, the bond between substrate and Bi is stronger than for NbO_x phase I, thereby resulting in a larger critical Bi coverage required for the phase transition. The fact that Bi atoms are more weakly bound on the NbO_x phase I is also evidenced by the fact that Bi(111) films on this surface break apart during the annealing process [see Fig. 4(b)]. Obviously, for the NbO_x phase II, where we observe the complete absence of a (110)-to-(111) transition, the bond between the substrate

and Bi layer at the interface is much stronger than for the other two Nb surfaces.

We speculate that the ordered oxygen rows of the NbO_x phase II which arrange along the $[\bar{1}\,1\,2]$ and $[\bar{1}\,1\,\bar{2}]$ directions [21], play an important role for this behavior. The absence of a phase transition possibly arises from interfacial Bi atoms which arrange in between the oxygen rows and thereby effectively pin the Bi(110) orientation. As a result the pinning might only be overcome at even higher Bi coverages exceeding 18 ML^{ps}. It may also be possible that the energy barrier for the transition is rather high and can only be overcome at a higher annealing temperature or longer annealing time. Further atomistic insight into the structural properties at the Bi–oxygen-terminated Nb(110) interface may be provided by other methods like surface-sensitive x-ray scattering, which is beyond the scope of this work.

VI. CONCLUSION

The data presented in this work show that the growth mode of Bi thin films on Nb(110) depends on the substrate's surface quality. For very thin Bi films on the NbO_x phase I we observe the coexistence of irregular clusters and (110)-terminated flat islands. The (110)-to-(111) transition already occurs at a Bi coverage of under 5 ML^{ps}. A completely different behavior can be observed for the higher ordered reconstructed NbO_x phase II, where no phase transformation could be observed and very smooth Bi(110) films remain stable up to Bi coverages of approximately 18 ML^{ps}. When the Nb(110) surface is cleaned from oxygen residues, the (110)-to-(111) phase transition occurs between 4.3 and 8.3 ML^{ps}, resulting in the smoothest Bi(111) film among all Nb surfaces. We envision that this behavior can be used to tune the orientation of the Bi films for almost arbitrary film thickness by adjusting the oxygen concentration of the Nb(110) surface.

[1] C. Nayak, S. H. Simon, A. Stern, M. Freedman, and S. Das Sarma, Non-Abelian anyons and topological quantum computation, Rev. Mod. Phys. **80**, 1083 (2008).

[2] D. Litinski, M. S. Kesselring, J. Eisert, and F. von Oppen, Combining Topological Hardware and Topological Software: Color-Code Quantum Computing with Topological Superconductor Networks, Phys. Rev. X **7**, 031048 (2017).

[3] B. Jäck, Y. Xie, J. Li, S. Jeon, B. A. Bernevig, and A. Yazdani, Observation of a Majorana zero mode in a topologically protected edge channel, Science **364**, 1255 (2019).

[4] S. Murakami, Quantum Spin Hall Effect and Enhanced Magnetic Response by Spin-Orbit Coupling, Phys. Rev. Lett. **97**, 236805 (2006).

[5] M. Wada, S. Murakami, F. Freimuth, and G. Bihlmayer, Localized edge states in two-dimensional topological insulators: Ultrathin Bi films, Phys. Rev. B **83**, 121310(R) (2011).

[6] Y. Ren, Z. Qiao, and Q. Niu, Topological phases in two-dimensional materials: A review, Rep. Prog. Phys. **79**, 066501 (2016).

[7] T. Hirahara, G. Bihlmayer, Y. Sakamoto, M. Yamada, H. Miyazaki, S. I. Kimura, S. Blügel, and S. Hasegawa, Interfacing 2D and 3D Topological Insulators: Bi(111) Bilayer on Bi_2Te_3, Phys. Rev. Lett. **107**, 166801 (2011).

[8] Z. F. Wang, M.-Y. Yao, W. Ming, L. Miao, F. Zhu, C. Liu, C. L. Gao, D. Qian, J.-F. Jia, and F. Liu, Creation of helical Dirac fermions by interfacing two gapped systems of ordinary fermions, Nat. Commun. **4**, 1384 (2013).

[9] F. Reis, G. Li, L. Dudy, M. Bauernfeind, S. Glass, W. Hanke, R. Thomale, J. Schäfer, and R. Claessen, Bismuthene on a SiC substrate: A candidate for a high-temperature quantum spin Hall material, Science **357**, 287 (2017).

[10] I. K. Drozdov, A. Alexandradinata, S. Jeon, S. Nadj-Perge, H. Ji, R. J. Cava, B. A. Bernevig, and A. Yazdani, One-dimensional topological edge states of bismuth bilayers, Nat. Phys. **10**, 664 (2014).

[11] F. Schindler, Z. Wang, M. G. Vergniory, A. M. Cook, A. Murani, S. Sengupta, A. Y. Kasumov, R. Deblock, S. Jeon, I. Drozdov, H. Bouchiat, S. Guron, A. Yazdani, B. A. Bernevig, and T. Neupert, Higher-order topology in bismuth, Nat. Phys. **14**, 918 (2018).

[12] H.-H. Sun, M.-X. Wang, F. Zhu, G.-Y. Wang, H.-Y. Ma, Z.-A. Xu, Q. Liao, Y. Lu, C.-L. Gao, Y.-Y. Li, C. Liu, D. Qian, D. Guan, and J.-F. Jia, Coexistence of topological edge state and superconductivity in bismuth ultrathin film, Nano Lett. **17**, 3035 (2017).

[13] F. Yang, J. Jandke, T. Storbeck, T. Balashov, A. Aishwarya, and W. Wulfhekel, Edge states in mesoscopic Bi islands on superconducting Nb(110), Phys. Rev. B **96**, 235413 (2017).

[14] X. Dong, Y. Li, J. Li, X. Peng, L. Qiao, D. Chen, H. Yang, X. Xiong, Q. Wang, X. Li, J. Duan, J. Han, and W. Xiao, Epitaxial growth and structural properties of Bi(110) thin films on $TiSe_2$ substrates, J. Phys. Chem. C **123**, 13637 (2019).

[15] T. Nagao, J. T. Sadowski, M. Saito, S. Yaginuma, Y. Fujikawa, T. Kogure, T. Ohno, Y. Hasegawa, S. Hasegawa, and T. Sakurai, Nanofilm Allotrope and Phase Transformation of Ultrathin Bi Film on Si(111)-7×7, Phys. Rev. Lett. **93**, 105501 (2004).

[16] Y. Lu, W. Xu, M. Zeng, G. Yao, L. Shen, M. Yang, Z. Luo, F. Pan, K. Wu, T. Das, P. He, J. Jiang, J. Martin, Y. P. Feng, H. Lin, and X. Wang, Topological properties determined by atomic buckling in self-assembled ultrathin Bi(110), Nano Lett. **15**, 80 (2015).

[17] S. Hatta, Y. Ohtsubo, S. Miyamoto, H. Okuyama, and T. Aruga, Epitaxial growth of Bi thin films on Ge(111), Appl. Surf. Sci. **256**, 1252 (2009).

[18] L. Peng, J.-J. Xian, P. Tang, A. Rubio, S.-C. Zhang, W. Zhang, and Y.-S. Fu, Visualizing topological edge states of single and

double bilayer Bi supported on multibilayer Bi(111) films, Phys. Rev. B **98**, 245108 (2018).

[19] O Hellwig and H Zabel, Oxygen ordering in Nb(110) films, Phys. B: Condens. Matter **336**, 90 (2003).

[20] K. Zhussupbekov, K. Walshe, S. I. Bozhko, A. Ionov, K. Fleischer, E. Norton, A. Zhussupbekova, V. Semenov, I. V. Shvets, and B. Walls, Oxidation of Nb(110): Atomic structure of the NbO layer and its influence on further oxidation, Sci. Rep. **10**, 3794 (2020).

[21] A. B. Odobesko, S. Haldar, S. Wilfert, J. Hagen, J. Jung, N. Schmidt, P. Sessi, M. Vogt, S. Heinze, and M. Bode, Preparation and electronic properties of clean superconducting Nb(110) surfaces, Phys. Rev. B **99**, 115437 (2019).

[22] P. Hofmann, The surfaces of bismuth: Structural and electronic properties, Prog. Surf. Sci. **81**, 191 (2006).

[23] Y. M. Koroteev, G. Bihlmayer, E. V. Chulkov, and S. Blügel, First-principles investigation of structural and electronic properties of ultrathin Bi films, Phys. Rev. B **77**, 045428 (2008).

[24] See Supplemental Material at http://link.aps.org/supplemental/10.1103/PhysRevMaterials.5.054801 for detailed information regarding STM data of various clean and oxygen-reconstructed Nb(110) surfaces, image processing procedures and additional LEED/STM data for higher coverages.

[25] We note that the subtle spot doubling or spot elongation recognizable in some LEED patterns is probably not related to rotated or shifted domains but to extrinsic effects. The most likely origin is a substantial bending of the single crystal surface which unavoidably builds up as multiple high-temperature flash cycles are performed during the cleaning process of the Nb(110) single crystal.

[26] W. R. Tyson and W. A. Miller, Surface free energies of solid metals: Estimation from liquid surface tension measurements, Surf. Sci. **62**, 267 (1977).

[27] S. Krause, L. Berbil-Bautista, T. Hänke, F. Vonau, M. Bode, and R. Wiesendanger, Consequences of line defects on the magnetic structure of high anisotropy films: Pinning centers on Dy/W(110), Europhys. Lett. **76**, 637 (2006).